

Effects of sea level rise on the salinity of Bahmanshir estuary

A. Etemad-Shahidi · M. S. Rohani ·
J. Parsa · C. Lemckert

Received: 23 February 2014/Revised: 30 June 2014/Accepted: 14 January 2015/Published online: 17 February 2015
© Islamic Azad University (IAU) 2015

Abstract Bahmanshir estuary, which is connected to the Persian Gulf, is one of the most important water resources in region. In this study, saltwater intrusion due to possible sea level rise in the Bahmanshir estuary was investigated. A one-dimensional hydrodynamic and water quality model was used for the simulation of the salinity intrusion and associated water quality, with measured field data being used for model calibration and verification. The verified model was then used as a virtual laboratory to study the effects of different parameters on the salinity intrusion. A coupled gas-cycle/climate model was used to generate the climate change scenarios in the studied area that showed sea level rises varying from 30 to 90 cm for 2100. The models were then combined to assess the impact of future sea level rise on the salinity distribution in the Bahmanshir estuary. Using important dimensionless numbers, a dimensionally homogenous equation was subsequently developed for the prediction of the salinity intrusion length, showing that the salinity intrusion length is inversely correlated with the discharge and directly with the sea level rise. In addition, the magnitude and frequency of the salinity standard violations at the pump station were predicted for 2100, showing that the salinity violations under climate

change effects can increase to 45 % of the times at this location. This reveals the importance of this type of approach for considering future infrastructure management.

Keywords Bahmanshir estuary · Salinity intrusion · Sea level rise · Climate change · Water quality

Introduction

Water level and its associated impact on the aquatic ecosystems are among the major problems to be faced by climate change occurrence (Abbaspour et al. 2012). Climate change and the global sea level rise (SLR) have been increased at an unprecedented rate over the past 100 years (e.g., Church and White 2006). Rahmstorf (2007) and Pfeffer et al. (2008) estimated the SLR to be on the order of 1 m by 2100, exceeding the estimates provided by the Intergovernmental Panel on Climate Change (IPCC 2007). This likely rise has prompted research into possible impacts on estuaries and associated infrastructure and management strategies. Estuaries, where freshwater from rivers mixes with saltwater from the oceans, are among the most productive environments on the earth. The intrusion of seawater in estuaries is an important phenomenon which occurs naturally and affects water quality (e.g., Etemad-Shahidi and Imberger 2002; Parsa et al. 2007). Saltwater intrusion into upper estuarine reaches, inflowing rivers and aquifers has been, and continues to be, one of the most important global challenges for coastal water-resource managers (Bear et al. 1999; Liu et al. 2011). Salinity is among common parameters that are known as governing flocculation factors in flocculation of metals during estuarine mixing in estuaries (Biati et al. 2010; Liu et al. 2012). Rising sea levels will result in a landward shift of the

A. Etemad-Shahidi (✉) · C. Lemckert
Griffith School of Engineering, Gold Coast Campus, Griffith
University, Gold Coast QLD 4222, Australia
e-mail: a.etemadshahidi@griffith.edu.au

M. S. Rohani
School of Civil Engineering, Iran University of Science and
Technology, P.O. Box 16765-163, Tehran, Iran

J. Parsa
Water Engineering Department, Agriculture Faculty, University
of Tabriz, Tabriz, Iran

estuarine salinity levels, thus threatening ecosystems and freshwater supplies in estuaries. SLR would turn backward the interface of saltwater–freshwater, and hence, the life of all species will be affected dramatically. Sea level rise, hereafter denoted as SLR, will play an important role in erosion processes which causes the land loss by losing the agricultural land, communication infrastructures and a wide range of biodiversity (Bhuiyan and Dutta 2012).

The Bahmanshir estuary is one of the main water supplies in the southwest of Iran (see Fig. 1). This estuary is the major source of water supply for Abadan and Khorramshahr area (Fig. 1). It supplies the agricultural and irrigation waters and also potable water for the large Abadan and Khorramshahr cities. In addition, this estuary acts as the major source of water for neighboring industries such as Abadan oil refinery and palm farms. In recent years, the salinity intrusion into Bahmanshir has increased due to the construction of multi-purpose dams in the upstream parts of Bahmanshir. The salinity intrusion has been monitored for a long time in the vicinity of Abadan city at a distance approximately 50–60 km from the mouth (Mahab-Sweco 1976). The intrusion of salinity in the Bahmanshir estuary and its effect on the agricultural and irrigational purposes is a very important issue. Spatial and temporal variability of the hydrodynamics and water quality in the Bahmanshir estuary is characterized by the tidal variation and freshwater in flow (Mahab-Sweco 1976). Estuarine responses to these variabilities are complex and difficult to understand. Hence, numerical models are generally used to predict their responses. Mahab-Sweco (1976), who used both a numerical model and Harlman's (1966) empirical model, was the first comprehensive study on the hydrodynamics and salinity intrusion in the Bahmanshir estuary. Shirdeli et al. (1998) and Parsa et al. (2005, 2007) used MIKE 11 and empirical models for this purpose as well and found that due to the well-mixed nature of Bahmanshir, one-dimensional models can be used to simulate the hydrodynamics and salinity distribution along this estuary.

The impact of SLR on estuarine intrusions has been studied for various locations. Sinha et al. (1997) studied the effects of SLR on the hydrodynamics and tidal circulation in the Hooghly estuary, Bay of Bengal, northeastern part of the Indian Ocean. Kont et al. (2003) studied SLR and its negative impacts in the coastal regions of Estonia. Conrads et al. (2010) estimated the salinity intrusion effects due to climate change on the Lower Savannah River estuary and found that the duration of salinity intrusion can increase substantially with an incremental SLR. However, the study of SLR on salinity intrusion has not been conducted in the Bahmanshir estuary yet, but is required due to the importance of the estuary to the local communities.

The aims of this study were (1) to find the influence of SLR and determination of the salinity intrusion length due to different SLR scenarios and (2) to suggest a simple equation for the prediction of the salinity intrusion length in the Bahmanshir estuary so that decision makers can plan future infrastructure (such as power station and water withdrawal systems). A one-dimensional hydrodynamics–water quality model was first verified to investigate the influence of forcing (tides, freshwater inflows) on the dynamic of the system. The verified model was then applied to study the implications of the SLR on the salinity distribution in the Bahmanshir estuary. This numerical investigation was conducted in 2011.

Materials and methods

Study area

Bahmanshir estuary, located in the southwest of Iran, is one of its main inland waterways. The length of Bahmanshir is about 78 km, and it accounts as the downstream branch of the Karun River. Another downstream branch of Karun is the Arvand estuary, which is extended along the Iran and Iraq border and is parallel to the Bahmanshir estuary and flows into the Persian Gulf. The Abadan Island is located between these estuaries and the Persian Gulf (Fig. 1).

The intrusion of seawater from the Persian Gulf to the Arvand, Bahmanshir and Karun rivers has been observed since 1925. This has caused concerns about freshwater consumers such as National Iranian Petroleum, cities of Abadan and Khorramshahr and also local farmers. After construction of several multi-purpose dams for electricity generation and flood control, salinity intrusion in the Bahmanshir has increased (Sazeh-Pardazi 1992). Due to the importance of water quality and especially salinity, the hydrodynamics and water quality of this estuary have been studied since more than three decades ago (Mahab-Sweco 1976), using both field measurements and numerical modeling.

The averaged cross-sectional area, width and depth of Bahmanshir are about 600 m², 200 m and 4 m, respectively. The annual discharge varies from 35 to 230 m³/s. The tidal range at the mouth is about 3.6 m at spring tide. During the dry seasons, when the Karun discharge is very low, the tidal influence may be observed as far as Ahvaz city, 120 km upstream of the Bahmanshir mouth. However, in normal conditions, the tidal influence only reaches about 48 km upstream (Parsa et al. 2007). The salinity at the mouth of the estuary varies between 35 and 40 ppt (Mahab-Sweco 1976).



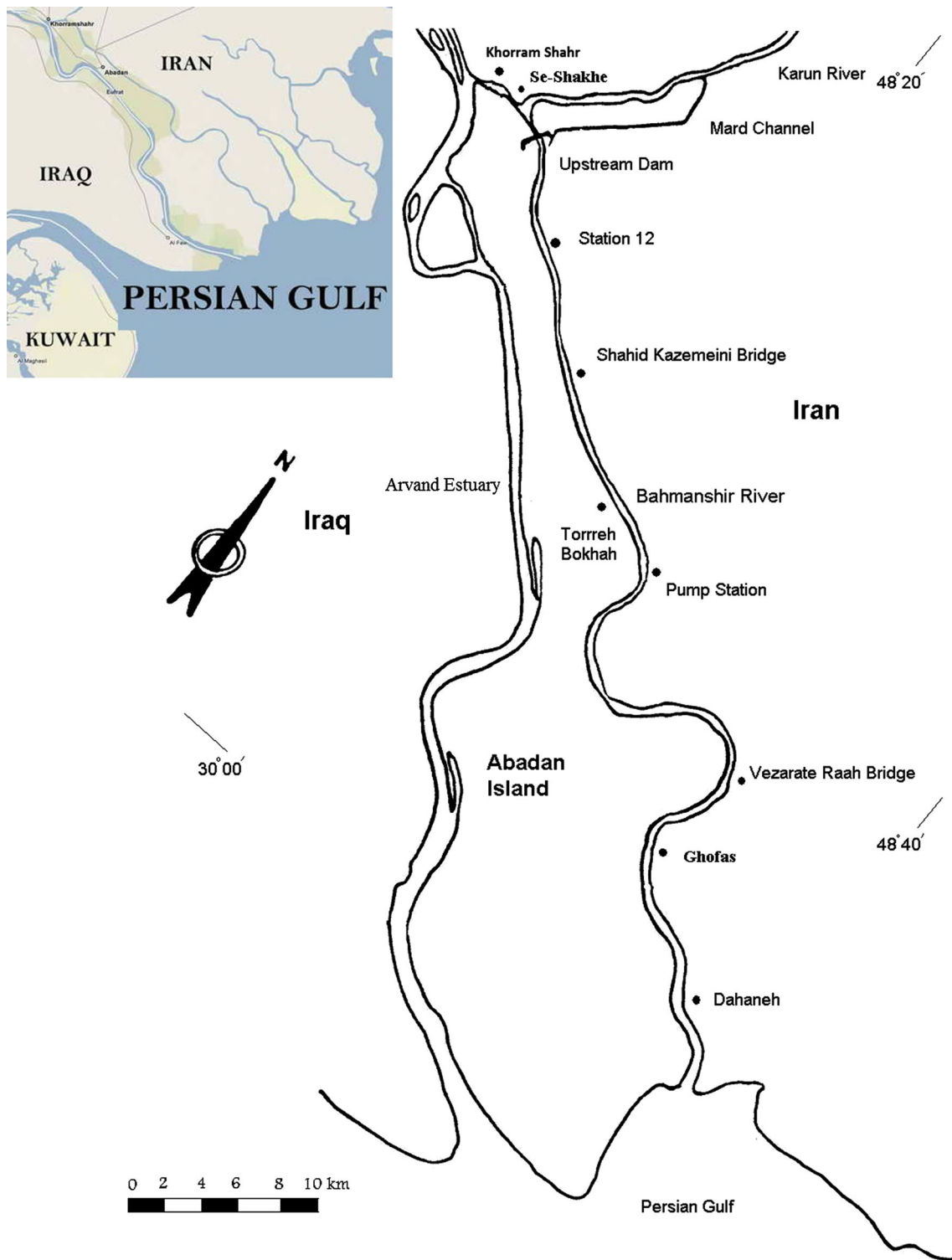


Fig. 1 Map of the study area (Parsa et al. 2007) and measurement stations

Model description

MIKE11 is the software for one-dimensional modeling of rivers, channels and irrigation systems (DHI 2009). It includes rainfall-runoff, advection–dispersion, morphology, water quality and sediment transport modules. It is capable of modeling water bodies with interconnected rivers, reservoirs and estuaries and has been successfully used to predict salinity and sediment transport in estuaries (e.g., Etemad-Shahidi et al. 2010). The model is based on an integrated modular structure with the hydrodynamic module as its core module and a number of add-on modules, each simulating certain phenomena in river systems. This model can be applied with fully dynamic descriptions and solves the laterally and vertically integrated equations of conservation of volume and momentum (the ‘Saint–Venant’ equations). The basic equations used in the model are as follows:

Conservation of mass:

$$\frac{\partial Q}{\partial x} + \frac{\partial A}{\partial t} = q \quad (1)$$

Conservation of momentum:

$$\frac{\partial Q}{\partial t} + \frac{\partial \alpha \frac{Q^2}{A}}{\partial x} + gA \frac{h_0}{\partial x} + g \frac{n^2 Q |Q|}{AR^{4/3}} = 0 \quad (2)$$

where Q is the discharge, A is the area of the cross section, q is the lateral discharge, t is the time, x is the distance along the river, α is the kinetic energy coefficient, h_0 is the elevation above an arbitrary datum, g is the gravity acceleration, n is the Manning coefficient, and R is the hydraulic or resistance radius.

The hydrodynamic module contains an implicit finite difference computation of unsteady flows in rivers and estuaries. The differential equations are solved using an efficient, accurate and robust implicit finite difference scheme known as the Abbott–Ionescu scheme (Abbott and Ionescu 1967). A six-point implicit staggered grid finite difference scheme is used for solving the equations. The details of the discretization method are given in Appendix.

The one-dimensional (vertically and laterally integrated) equation for the conservation of mass of a substance in solution, i.e., the one-dimensional advection–dispersion equation, is

$$\frac{\partial AC}{\partial t} + \frac{\partial QC}{\partial t} - \frac{\partial}{\partial x} \left(AD \frac{\partial C}{\partial x} \right) = -AK_d C + C_2 q \quad (3)$$

where C is the concentration, D is the longitudinal dispersion coefficient, K_d is the linear decay coefficient, and C_2 is the source/sink concentration. The dispersion coefficient was specified as a function of the flow velocity calculated by the following equation (Bhuiyan and Dutta 2012; Etemad-Shahidi and Taghipour 2012):

$$D = aU^b \quad (4)$$

where U is the cross-sectionally averaged flow velocity and a and b are constant values that are approximated by model calibration.

This module requires output from the hydrodynamic module in terms of discharge, water level, cross-sectional area and hydraulic radius. The advection–dispersion equation is solved using a fully time, and space-centered implicit finite difference scheme, which is unconditionally stable and has a negligible artificial dispersion (DHI 2009).

Calibration and verification of the model

The Bahmanshir is a well-mixed estuary, and a one-dimensional model can be used (Mahab-Sweco 1976; Shirdeli et al. 1998; Parsa et al. 2007; Bhuiyan and Dutta 2012). Although it may be some stratification in the estuary during wet season, the hydrodynamic and salinity distribution responses of the estuary under the effects of climate change were evaluated only under the worst scenario which is the well-mixed conditions of the estuary. To model this water body, 66 km of the estuary was considered and divided into segments with about 1 km length. To calibrate the MIKE hydrodynamic module, simulations were conducted using simultaneous time series for upstream discharge at station 12 (km 7 from the upstream) and

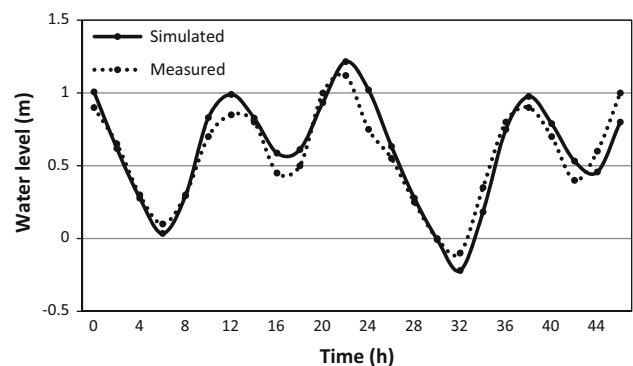


Fig. 2 Comparison between the simulated and measured water levels, km 15 (Vezerate Rah Bridge), April 4–5

downstream tidal level measurements at Dahaneh station (km 73) as the boundary conditions (Fig. 1). The model requires a warm-up period, during which time the effects of initial conditions are washed out. Two tidal cycles (50 h) were found adequate for the model to warm-up and used time step was 600 s.

The Manning coefficient was determined by minimizing the difference between the measured and predicted water levels at 15 km upstream from the mouth. A Manning coefficient of 0.018 was obtained with a relative error of 8 % between the simulated and measured values of water levels (Fig. 2). In order to use all the available field data and showing the robustness of the model, measurements from different stations have been used for calibration and verification of hydrodynamics and advection–dispersion modules of the model. For the verification of the hydrodynamic module, another simulation was performed along the estuary and the obtained results were compared with the field data collected at a station 53 km from the mouth. The relative error between simulated water levels and observed values in this station was about 10 % (Fig. 3). Furthermore, simulated velocities were compared with the field data collected at the Ghofas station. The relative error between simulated and observed values in this station was about 19 % (Fig. 4). These results showed that the model worked at a satisfactory level, compared with the similar numerical studies carried out in this area (e.g., Mahab-Sweco 1976; Parsa et al. 2007; Etemad-Shahidi et al. 2014).

For simulation of the advection and dispersion processes, measured salinity of 1.2 ppt (part per thousand) was

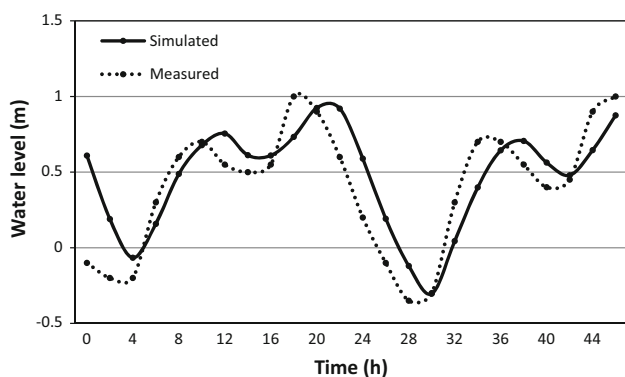


Fig. 3 Comparison between the simulated and measured water levels, km 53 (Torreh Bokhah), April 4–5

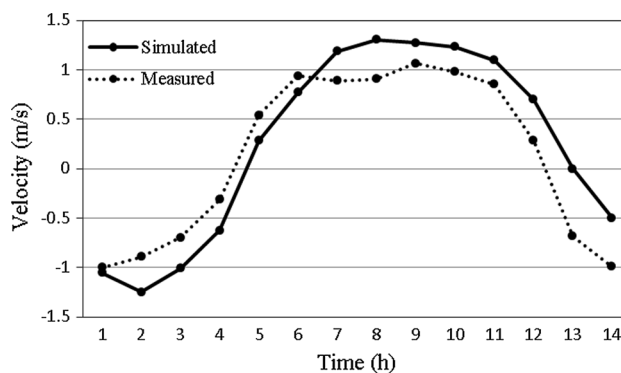


Fig. 4 Comparison between the simulated and measured velocities, Ghofas

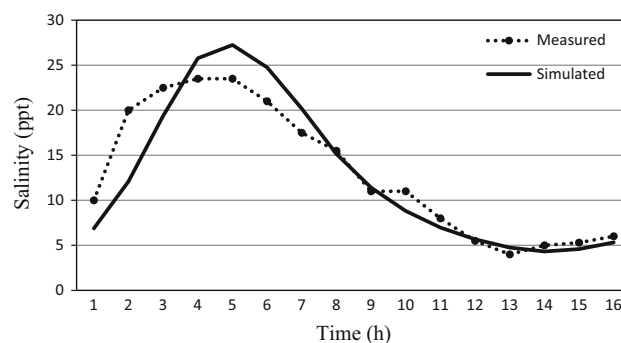


Fig. 5 Comparison between simulated and measured salinities, Ghofas

used as the upstream boundary condition. The measured salinity at the Persian Gulf, i.e., 38 ppt, was imported to the model as the downstream boundary condition. To calibrate the model, a dispersion coefficient, as the calibration parameter, was determined by minimizing the differences between measured and simulated salinity at Ghofas (23 km from the mouth). In this way, the dispersion coefficient was calibrated, by optimizing the constant values in Eq. (4), as follows:

$$D = 400 U \tag{5}$$

The relative error between the measured and simulated salinities was 9 % which is satisfactory (Fig. 5).

The verified model was then used for simulating the effects of SLR on the salinity structure. Noting that the dispersion coefficient is not constant and depends on velocity, Eq. 5 was used for the estimation of longitudinal dispersion coefficients in different scenarios.

Sea level rise scenarios

A simple climate model called the Model for the Assessment of Greenhouse-gas Induced Climate Change (MAGICC) and a regional climate change database SCENario GENerator (SCENGEN) were used to generate the required scenarios. These models have been developed by the Climatic Research Unit, University of East Anglia, UK. MAGICC/SCENGEN is a coupled gas-cycle/climate model that drives a spatial climate change SCENGEN. MAGICC has been one of the primary models used by IPCC since 1990 to produce predictions of the future global mean temperature and SLR. The climate model in MAGICC is an upwelling-diffusion, energy-balance model that produces global and hemispheric mean temperature output together with results for oceanic thermal expansion (Wigley 2008). The MAGICC climate model is coupled interactively with a range of gas-cycle models that give projections for the concentrations of the key greenhouse gases. Climate feedbacks on the carbon cycle are therefore accounted for (Wigley 2008).

Greenhouse gas emission scenarios are used in the MAGICC model. These scenarios are projections of future greenhouse gas emissions derived from using different assumptions about human activities, policies and technological applications. The projections show how sensitive emissions are to different parameters such as the population growth and changes in the patterns of consumption (Legget et al. 1992). These scenarios are grouped into four scenario families (A1, A2, B1 and B2). The A1 storyline assumes a very rapid economic growth, a global population that peaks in the mid-century and the rapid introduction of new and more efficient technologies in the world. A1 is divided into three groups that describe alternative directions of technological change: fossil intensive (A1FI), non-fossil energy resources (A1T) and a balance across all sources (A1B). B1 describes a convergent world, with the same global population as A1 (IPCC 2007), but with more rapid changes in economic structures toward a service and information economy. B2 describes a world with intermediate population and economic growth, emphasizing local solutions to economic, social and environmental sustainability. A2 describes a very heterogeneous world with high population growth, slow economic development and technological change. No likelihood has been attached to any of the SRES scenarios (IPCC 2007).

MAGICC uses some parameters as inputs in the modeling procedure. The most important of them is the climate sensitivity, i.e., the eventual global warming which would occur following the doubling of greenhouse gas concentrations (Kont et al. 2003; Roshan et al. 2010). To estimate the maximum possible SLR, extreme values of the parameters were used. The MAGICC outputs according to the maximum emission scenario show the increase in the global annual mean air temperature and sea level rise. Using the A1FI emission scenario, a warming by the range of 2.5–6.5 °C and sea level rises from 30 to 90 cm were projected for 2100. The climate change scenarios for the region were created using SCENGEN, a simple software tool that enables one to use the results from the MAGICC and general circulation model (GCM) experiments. These are combined with observed global and regional climatologies to construct a range of geographically explicit future climate change scenarios for every region of the world. The SCENGEN allows one to explore consequences for these scenarios by applying different assumptions about climate system parameters and emission scenarios and by selecting results from different GCM experiments (Rotmans et al. 1994; Hulme et al. 1995). No systematic investigation has been conducted on the effects of climate change on the river discharge in this area. However, the results of SCENGEN showed that the precipitation in this area will reduce by about 10 %. To mimic this, a 10 % reduction in discharge was assumed for dry seasons. SCENGEN shows that the precipitation in this area will reduce by about 10 %. According to the climate change scenario results, the projected values of the sea level rise projections are 30 cm as the minimum to 60 cm on average and a maximum of 90 cm in 2100. The SLR values derived from this model were then applied at the downstream boundary of the model. Four tidal constituents, i.e., M_2 (Principal lunar semidiurnal), S_2 (Principal solar semidiurnal), K_1 (Lunisolar diurnal) and O_1 (Principal lunar diurnal) were specified to generate time series of water surface elevations (summation of constituents) as the open boundary conditions at the mouth of the estuary. Each of these tidal constituents represents a periodic change or variation in the relative positions of the Earth, Moon and Sun. The period of each constituent is the time required for the phase to change through 360° and is the cycle of the astronomical condition represented by the constituent (www.tidesandcurrents.noaa.gov). It was assumed that these constituent phases do not change with time.



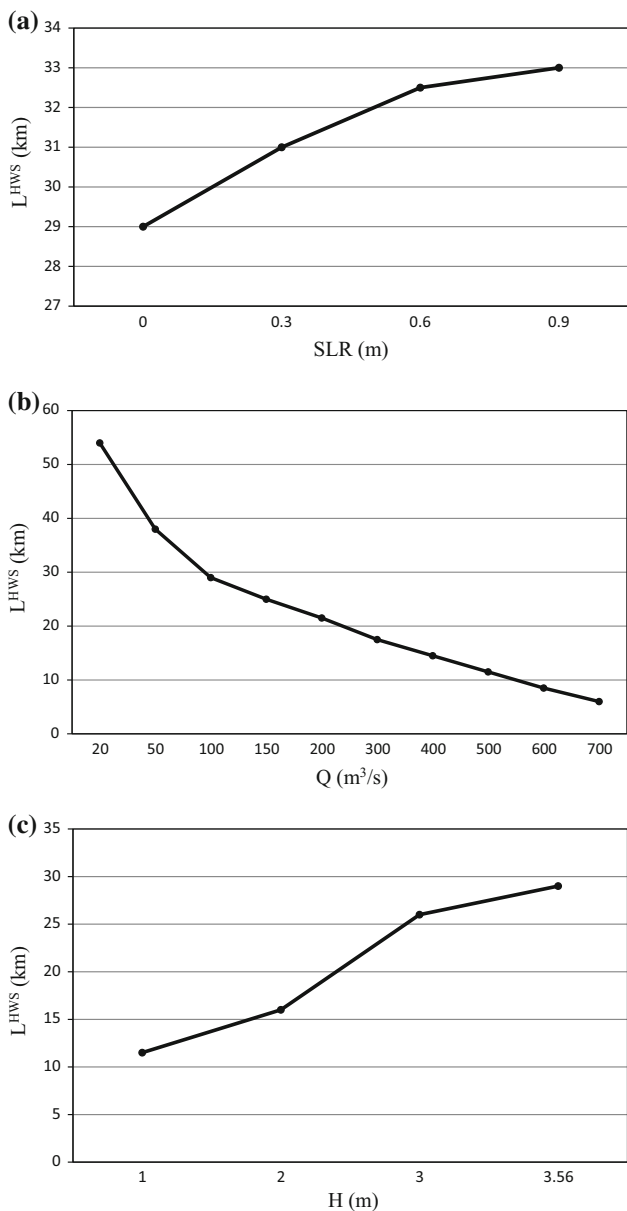


Fig. 6 **a** Variations of the salinity intrusion length versus sea level rise, **b** variations of the salinity intrusion length versus freshwater discharge and **c** variations of the salinity intrusion length versus tidal range

Results and discussion

Effect of important parameters

The influences of the important parameters on the salinity intrusion are described here. Figure 6a–c shows the effects of SLR, riverine discharge (Q) and tidal range (H) on the

Table 1 Salinity intrusion lengths (km) due to different sea level rise scenarios and freshwater discharges

Q (m^3/s)	20	100	500	700
L (Base case)	54	29	11.5	6
L (SLR30)	55.8	31	14	8.5
L (SLR60)	57.3	32.5	15.2	9.4
L (SLR90)	58.7	33	16.5	10.7

salinity intrusion length at high water slack (L^{HWS}) in the Bahmanshir estuary. For this study, the salinity intrusion length is considered as the distance from the mouth to the point where the salinity becomes 1 ppt more than the river water salinity (Van der Tuin 1991; Parsa et al. 2007).

The effect of the SLR on the salinity intrusion is displayed in Fig. 6a for SLR scenarios of 0.3, 0.6 and 0.9 m and the base case (no SLR). As the sea level increases, the salinity intrusion length increases in the Bahmanshir estuary. Figure 6a indicates that, assuming other parameters remain constant ($Q = 100 m^3/s$ and $H = 3.56 m$), by a SLR of 0.9 m, the length of salinity intrusion increases approximately 4 km. SLR increases the depth of the estuary, and as a consequence, the discharge of tidal flow becomes higher and the salinity intrusion increases. It should be noted that change in the salinity due to the SLR is not uniform within the estuary. For example, due to 60 cm SLR, the salinity levels at the stations 12, Shahid Kazemieni bridge (km 15) and Dahaneh stations (Fig. 1), change insignificantly, while the maximum salinity increase (6 ppt) occurs about at km 54 from upstream. The response of the salinity intrusion length to the variation of river discharge was studied for flow ranging from $Q = 20 m^3/s$ to $700 m^3/s$. This range of river discharge is selected based on the historical records of the river discharge in different seasons (Sazeh-Pardazi 1992). Figure 6b illustrates the salinity intrusion lengths versus the river discharge. Increased freshwater discharge pushes the limits of salt intrusion toward the river mouth. When the river discharge is decreased as a consequence of the 10 % reduction in precipitation resulting from climate change scenario, the salinity intrusion length increases. Similarly, other studies also revealed the inverse relationship between salinity intrusion length and freshwater discharge. For example, recent numerical studies of Liu and Liu (2014) in Wu River system in Taiwan showed that the salinity intrudes further during dry seasons. Similarly, Rice et al. (2012) found that in Chesapeake Bay, the salt intrusion is enhanced in dry periods compared with that of typical periods. The observed inverse relationship between salinity

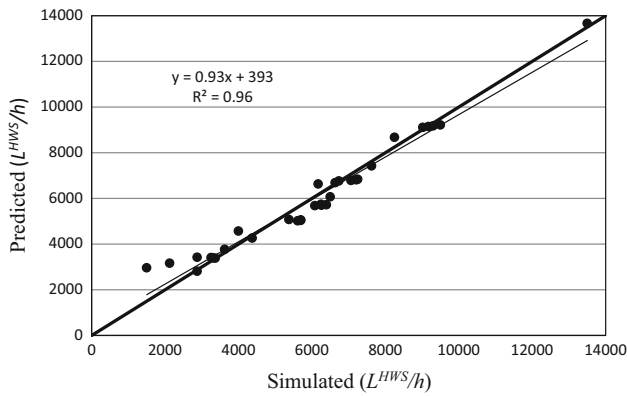
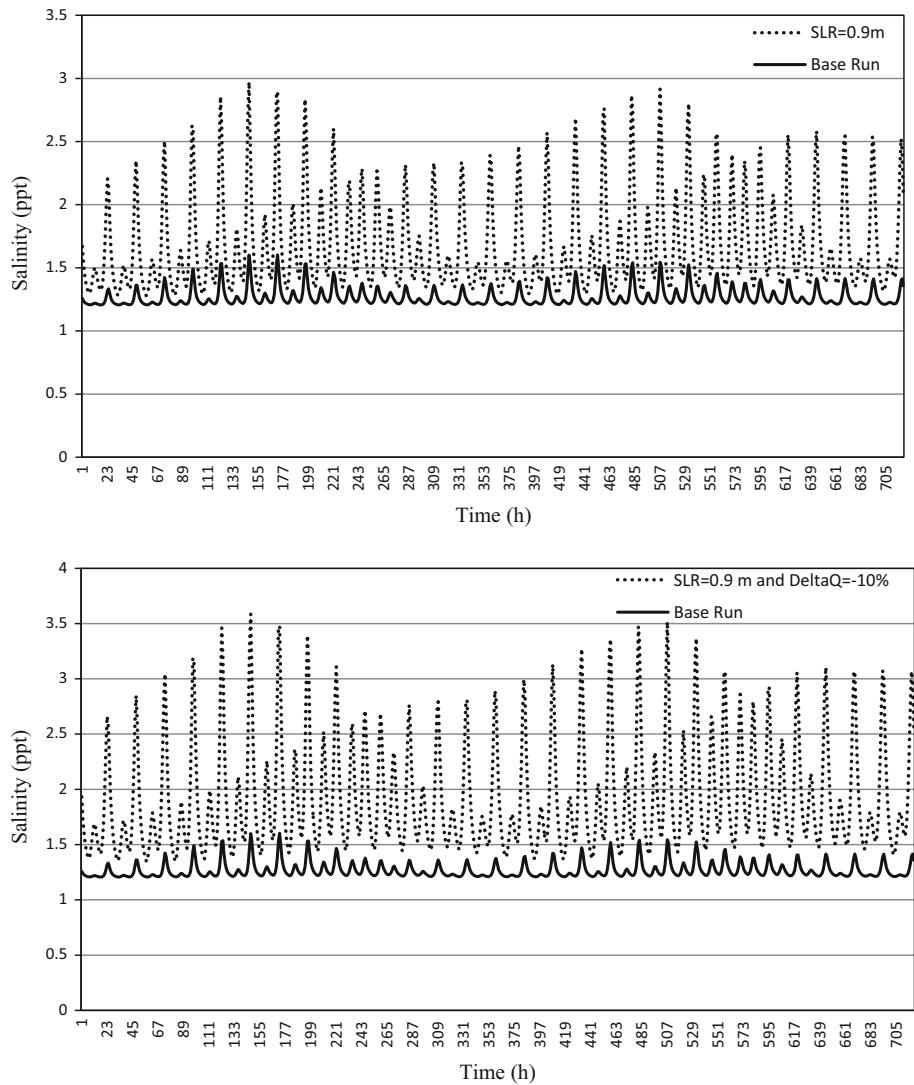


Fig. 7 Comparison between the simulated and predicted dimensionless salinity intrusion lengths ($R^2 = 0.96$, number of data points is 30 and $m = 0.93$)

intrusion length and discharge is also in line with the results of previous studies in which the relationship between salinity intrusion length and river discharge is reported as $L \sim (Q^{-0.2} \text{ to } Q^{-0.33})$ (Oey 1984; Monismith et al. 2002; Zahed et al. 2008; Parsa and Etemad-Shahidi 2011). According to Fig. 6b, at the low flow ($Q = 20 \text{ m}^3/\text{s}$), the length of salinity intrusion is 54 km. When the discharge is equal to $700 \text{ m}^3/\text{s}$ (high flow), salinity intrusion length is only 6 km.

Another important factor on the salinity intrusion is the tidal range. The model was also run for different values of tidal ranges assuming other parameters being constant as the base case. After developing time series of downstream boundary conditions using different tidal levels, three scenarios of SLR were considered and the relevant water

Fig. 8 a Salinity time series at pump station for base run and SLR = 0.9 m, **b** salinity time series at pump station for base run and SLR = 0.9 m plus 10 % discharge reduction



level rises were added to the developed tidal level time series. Figure 6c indicates that the salinity intrusion length increases with the increase in the tidal range. The minimum tidal range occurs in neap tides when the tidal range is equal to 1 m, and the salinity intrusion length is 12 km (for $Q = 100 \text{ m}^3/\text{s}$). During spring tides, the tidal range and salinity intrusion length are 3.56 m and 29 km, respectively. This is in agreement with the previous findings of, e.g., Van der Burgh (1972) and Parsa and Etemad-Shahidi (2011), in which $L \sim H^{0.45-0.5}$. The amplitude of tidal velocity can be considered as a linear function of tidal range (Ippen 1966; Prandle 2004). As the tidal range increases, the tidal velocity and hence the salinity intrusion length increase as well.

The lengths of salinity intrusion due to SLR scenarios under different inflow conditions are tabulated in Table 1. It shows (under different discharges) when the sea level rises, the length of the salinity intrusion increases. The increase in the salinity intrusion length depends more on the SLR rather than the river discharge. In other words if the sea level rises by 90 cm (worst case), the length of salinity intrusion increases by about <5 km in all considered flow conditions.

Development of an equation for the salinity intrusion length

The most important task in developing an equation for the prediction of salinity intrusion length is to find the governing parameters to be included in the equation. A simple function that can consider is the variability of the governing parameters assuming constant depth, roughness, tidal period and density difference is as follows (see also Parsa and Etemad-Shahidi 2010; Etemad-Shahidi et al. 2009a, 2011):

$$L^{\text{HWS}} = f(Q, H, \text{SLR}) \tag{6}$$

The parameters involved in the salinity intrusion length were correlated through dimensional analysis. Different combinations of these parameters were tested for developing the equations. Here, the simplest and most accurate equation is presented. The most important dimensionless parameters were found to be $Q/(A\sqrt{gh})$ and H/h , (Parsa and Etemad-Shahidi 2011) where h is the depth. To show the effects of SLR in different scenarios, h can be defined as $h = h_0 + \text{SLR}$. Equation (6) may be reduced in terms of a set of dimensionless parameters as

$$L^{\text{HWS}}/h = f\left(Q/(A\sqrt{gh}), H/h\right) \tag{7}$$

A power law form of Eq. (7) may be expressed as

$$L^{\text{HWS}}/h = a\left(Q/(A\sqrt{gh})^b (H/h)^c\right) \tag{8}$$

where a is the coefficient and b and c are the exponents of the equation. This power law form is also supported by the previous findings (e.g., Prandle 2004; Zahed et al. 2008).

To develop the relationship between dimensionless parameters, the verified model was used to simulate several scenarios with different discharge, tidal ranges and sea level rises. Then, the obtained results were used as the data set of salinity intrusion lengths to develop the equation. The following equation was obtained by nonlinear multi-variable regression:

$$\left(L^{\text{HWS}}/h\right) = 1366\left(Q/(A\sqrt{gh})\right)^{-0.43} (H/h)^{0.7} \tag{9}$$

$(R = 0.98)$

where R is the correlation coefficient. Equation 9 indicates that H is very important and salinity intrusion length is very sensitive to the tidal range. The power of h in this equation is 0.5, which is supported by the findings of Hong and Shen (2012) in Chesapeake Bay. In brief, the salinity intrusion length is very sensitive to any SLR as it impacts directly on the average depth.

Figure 7 displays the comparison between the numerically simulated salinity intrusion lengths and the predicted ones by Eq. 9. As seen, most of the data points are close to the line of the perfect agreement, indicating that Eq. 9 can be used as a rapid assessment tool to assist managers in decision-making processes.

Effect of sea level rise on the pump station

Salinity is an important water quality parameter for both drinking and agricultural purposes (e.g., Rice et al. 2012; Etemad-Shahidi et al. 2009b). At the pump station (32 km upstream from the mouth), the salinity must be <1.6 ppt to comply with the water quality standards. The frequency and duration of the salinity violations at this station are of great concern. Time series of the salinity due to a 0.9-m SLR alone, and 0.9 m SLR and 10 % reduction of freshwater because of the precipitation reduction, are shown in Fig. 8a, b, respectively. The warm-up time was found to be two tidal cycles (about 50 h), and the results of 1-month simulation period at the low flow ($Q = 25 \text{ m}^3/\text{s}$) showed that the salinity does not exceed 1.6 ppt in the base case (Fig. 8). However, a 0.9-m SLR increases the violations of salinity standard to 45 % of the time. SLR with the reduction of the freshwater flow increases this to 72 % of the time with severe consequences for the agricultural uses in this area. These results are consistent with the findings of Rice et al. (2012) in James River, USA, where they noticed that number of days with violation of salinity

limit for drinking purpose will be more than two times higher due to the SLR.

The results of this study enable water-resource managers to plan mitigation strategies to minimize the effects of climate change and associated SLR. These strategies may include timing of withdrawals during ebb tides, construction of temporary barriers, increased storage of freshwater, timing of larger releases of regulated flows to push the saltwater front downstream, and the mixing of brackish water with freshwater from an alternative source such as neighboring river (Arvand) or groundwater (Conrads et al. 2010). As a summary, the deposition of sediments due to the SLR will cause the rising of the estuary bed to restore the equilibrium state. These two events happen in different timescales, and the morphological changes occur by a remarkable lag time after hydrological changes. Hence, the present work shows the worst conditions of salinity intrusion in this estuary as a probable case.

Conclusion

In this study, the saltwater intrusion due to the SLR was studied for the Bahmanshir estuary. A numerical model was first calibrated and verified using field data. Then, the verified model was used to study the effects of different parameters on the salinity intrusion. More specifically, the model was used to assess the impact of the SLR on the salinity distribution in the Bahmanshir estuary. To generate the SLR scenarios, a simple climate model (MAGICC) was used. Using the A1FI emission scenario, sea level rises from 30 to 90 cm were projected for 2100. The verified model was run for a range of several SLR scenarios. A simple equation was derived to predict the salinity intrusion length in the Bahmanshir estuary using the obtained results. To achieve this goal, dimensionless parameterization and nonlinear multiple regression analysis were used. It was also found that a SLR of 0.9 m increases the salinity violation to 45 % of the times at a pump station located 32 km from upstream, thus requiring managers to consider future management schemes to minimize the impact of enhanced salinity levels at the station. The approach used here, with associated morphological effects of climate changes which is not considered here, can certainly be applied to other estuarine systems to assist their future management plans.

Acknowledgments The authors are grateful to the DHI for its invaluable support and providing the MIKE11 model, and the Khuzestan Water and Wastewater Company for providing the field data.

Appendix

Numerical discretization of the governing equations.

Conservation of mass:

$$\frac{\partial Q}{\partial x} + b_s \frac{\partial h}{\partial t} = q \quad (10)$$

where b_s is the storage width

The derivatives of Eq. 10 can be shown as

$$\frac{\partial Q}{\partial x} \approx \frac{\frac{(Q_{j+1}^{n+1} + Q_{j+1}^n)}{2} - \frac{(Q_{j-1}^{n+1} + Q_{j-1}^n)}{2}}{\Delta 2x_j} \quad (11)$$

$$\frac{\partial h}{\partial t} \approx \frac{(h_j^{n+1} - h_j^n)}{\Delta t} \quad (12)$$

b_s in Eq. 10 can be approximated as

$$b_s = \frac{A_j + A_{j+1}}{\Delta 2x_j} \quad (13)$$

Inserting the derivatives in Eq. 10 yields

$$\alpha_j Q_{j-1}^{n+1} + \beta_j h_j^{n+1} + \gamma_j Q_{j+1}^{n+1} = \delta_j \quad (14)$$

Momentum conservation equation:

$$\frac{\partial Q}{\partial t} \approx \frac{Q_j^{n+1} - Q_j^n}{\Delta t} \quad (15)$$

$$\frac{\partial \left(\alpha \frac{Q^2}{A} \right)}{\partial x} \approx \frac{\left[\alpha \frac{Q^2}{A} \right]_{j+1}^{n+1/2} - \left[\alpha \frac{Q^2}{A} \right]_{j-1}^{n+1/2}}{\Delta 2x_j} \quad (16)$$

$$\frac{\partial h}{\partial x} \approx \frac{\frac{(h_{j+1}^{n+1} + h_{j+1}^n)}{2} - \frac{(h_{j-1}^{n+1} + h_{j-1}^n)}{2}}{\Delta 2x_j} \quad (17)$$

Inserting these derivatives' in the conservation of momentum equation yields

$$\alpha_j h_{j-1}^{n+1} + \beta_j Q_j^{n+1} + \gamma_j h_{j+1}^{n+1} = \delta_j \quad (18)$$

where

$$\alpha_j = f(A) \quad (19)$$

$$\beta_j = f(Q_j^n, \Delta t, \Delta x, C, A, R) \quad (20)$$

$$\gamma_j = f(A) \quad (21)$$

$$\delta_j = f\left(A, \Delta x, \Delta t, \alpha, q, v, \theta, h_{j-1}^n, Q_{j-1}^{n+1/2}, Q_j^n, h_{j+1}^n, Q_{j+1}^{n+1/2}\right) \quad (22)$$

Therefore, the momentum and mass conservation equations can be written in a similar form as follows

$$\alpha_j Z_{j-1}^{n+1} + \beta_j Z_j^{n+1} + \gamma_j Z_{j+1}^{n+1} = \delta_j \quad (23)$$

References

- Abbaspour M, Javid AH, Mirbagheri SA, Givi FA, Moghimi P (2012) Investigation of lake drying attributed to climate change. *Int J Environ Sci Technol* 9(2):257–266
- Abbott MB, Ionescu F (1967) On the numerical computation of nearly-horizontal flows. *J Hydraul Res* 5:97–117
- Bear J, Cheng S, Sorek D, Ouazar I, Herrera EDS (1999) *Seawater intrusion in coastal aquifers—concepts, methods and practices*. Kluwer Academic Publishers, Dordrecht, pp 152–171
- Biati A, Karbassi AR, Hassani AH, Monavari SM, Moattar F (2010) Role of metal species in flocculation rate during estuarine mixing. *Int J Environ Sci Technol* 7(2):327–336
- Bhuiyan JAN, Dutta D (2012) Assessing impacts of sea level rise on river salinity in the Gorai river network, Bangladesh. *Estuar Coast Shelf Sci* 96:219–227
- Church JA, White NJ (2006) A 20th century acceleration in global sea level rise. *Geophys Res Lett* 33:1–4
- Conrads PA, Roehl EA, Daamen RC et al (2010) Estimating salinity intrusion effects due to climate change on the lower Savannah river estuary. Paper presented at the South Carolina environmental Conference, North Myrtle Beach, South Carolina, Mar 2010
- DHI Software Group (2009) MIKE 11 reference manual. Danish Hydraulic Institute, Denmark
- Etemad-Shahidi A, Imberger J (2002) Anatomy of turbulence in a narrow and strongly stratified estuary. *J Geophysical Res Ocean* 107:701–716
- Etemad-Shahidi A, Parsa J, Hajiani M (2009). Salinity intrusion length: comparison of different approaches. *Proceedings of the Institution of Civil Engineers—Maritime Engineering* 164:33–42
- Etemad-Shahidi A, Afshar A, Alikia H, Moshfeghi H (2009b) Total dissolved solid modeling; Karkheh reservoir case example. *Int J Environ Res* 3:671–680
- Etemad-Shahidi A, Shahkolahi A, Liu WC (2010) Modeling of hydrodynamics and cohesive sediment transport in an estuarine system: case study in Danshui river. *Environ Model Assess* 15:261–271
- Etemad-Shahidi A, Parsa J, Hajiani M (2011) Salinity intrusion length: comparison of different approaches. *PICE Marit Eng* 164:32–42
- Etemad-Shahidi A, Taghipour M (2012) Predicting longitudinal dispersion coefficient in natural streams using M5' model tree, ASCE. *J Hydraul Eng* 138:542–554
- Etemad-Shahidi A, Pirnia M, Moshfeghi H, Lemckert C (2014) Investigation of hydraulics transport time scales within the Arvand River estuary. *Hydrol Process*. doi:10.1002/hyp.10095
- Harlman DRF (1966) Salinity intrusion in estuaries. In: Ippen AT (ed) *Estuary and coastline hydrodynamics*. McGraw-Hill, New York, pp 598–629
- Hong B, Shen J (2012) Responses of estuarine salinity and transport processes to potential future sea-level rise in the Chesapeake Bay. *Estuar Coast Shelf Sci* 104–105:33–45
- Hulme M, Raper SCB, Wigley TML (1995) An integrated framework to address climate change (ESCAPE) and further developments of the global and regional climate modules (MAGICC). *Energy Policy* 23:347–356
- IPCC (2007) *Climate change 2007. The fourth assessment report (AR4) of the United Nations Intergovernmental Panel on Climate Change (IPCC)*
- Ippen AT (1966) *Estuary and coastline hydrodynamics*. McGraw-Hill, New York, pp 385–401
- Kont A, Jaagus J, Aunap R (2003) Climate change scenarios and the effect of sea-level rise for Estonia. *Glob Planet Change* 36:1–15
- Leggett J, Pepper WJ, Swart RJ (1992) Emission scenarios for the IPCC: an update. In: Houghton JT, Callander BA, Varney SK (eds) *Climate change 1992: the supplementary report to the IPCC scientific assessment*. Cambridge University Press, Cambridge, pp 75–95
- Liu WC, Chen WB, Hsu M-H (2011) Influences of discharge reductions on salt water intrusion and residual circulation in Danshuei River. *J Mar Sci Technol* 19:596–606
- Liu WC, Chen W-B, Chnag YP (2012) Modeling the transport and distribution of lead in tidal Keelung River estuary. *Environ Earth Sci* 65:39–47
- Liu WC, Liu HM (2014) Assessing the impacts of sea level rise on salinity intrusion and transport time scales in a tidal estuary, Taiwan. *Water* 6:324–344
- Mahab-Sweco (1976) *Abadan Island and Khorramshahr water supply and irrigation project hydraulic condition and salt water mathematical model studies*. Khuzestan Water and Power Organization, Technical Report, 184p, Iran
- Monismith S, Kimmerer W, Burau J, Stacey M (2002) Structure and flow-induced variability of the subtidal salinity field in Northern San Francisco Bay. *J Phys Oceanogr* 32:3003–3019
- Oey L (1984) On steady salinity distribution and circulation in partially mixed and well mixed estuaries. *J Phys Oceanogr* 32:629–645
- Parsa J, Etemad-Shahidi A, Hosseiny S, Yeganeh-Bakhtiary A (2007) Evaluation of computer and empirical models for prediction of salinity intrusion in the Bahmanshir estuary. *J Coast Res Special Issue* 50:658–662
- Parsa J, Etemad-Shahidi A, Jabbari E (2005) On the salinity intrusion empirical models in estuaries and their application in the Bahmanshir estuary. XXXI IAHR Conference (Seoul, Korea) 4553–4560
- Parsa J, Etemad-Shahidi A (2010) Prediction of tidal excursion length in estuaries due to the environmental changes. *Int J Environ Sci Technol* 7(4):675–686
- Parsa J, Etemad-Shahidi A (2011) An empirical model for salinity intrusion in alluvial estuaries. *Ocean Dyn* 61:1619–1628
- Pfeffer WT, Harper JT, O'Neel S (2008) Kinematic constrains on glacier contributions to 21st-century sea-level rise. *Science* 321:1340–1343
- Prandle D (2004) Saline intrusion in partially mixed estuaries. *Estuar Coast Shelf Sci* 59:385–397
- Rahmstorf S (2007) A semi-empirical approach to projecting future sea level rise. *Science* 315:368–370
- Rice KC, Hong B, Shen J (2012) Assessment of salinity intrusion in the James and Chickahominy Rivers as a result of simulated sea level rise in Chesapeake Bay, East Coast, USA. *J Environ Manag* 111:61–69
- Roshan GhR, Ranjbar F, Orosa JA (2010) Simulation of global warming effect on outdoor thermal comfort conditions. *Int J Environ Sci Technol* 7(3):571–580
- Rotmans J, Hulme M, Downing TE (1994) Climate change implications for Europe: an application of the ESCAPE model. *Glob Environ Change* 4:97–124
- Sazeh-Pardazi (1992) *Salinity intrusion in Bahmanshir estuary*. Technical Report 158p, Iran
- Sinha PC, Rao YR, Dube SK, Murty TS (1997) Effect of sea level rise on tidal circulation in Hooghly Estuary, Bay of Bengal. *Mar Geod* 20:341–366
- Shirdeli A, Shafaei M, Shafaei M (1998) Optimising salinity control structure of Bahmanshir River. *Proceedings of the 3rd*



- International Conference on Coasts, Ports and Marine Structures ICOPMAS (Tehran, Iran), 415–430
- Van der Burgh P (1972). Ontwikkeling van een methods voor het voorspellen van Zoutverde Lingen in estuaria, Kanalen en Zeeen. Rijkswaterstaat Rapport, 10–72
- Van der Tuin H (1991) Guidelines on the study of seawater intrusion into rivers. Prepared for the International Hydrological Programme by the Working Group of Project 4.4b (IHP-III), UNESCO
- Wigley TML (2008). MAGICC/SCENGEN 5.3: USER MANUAL (version 2). NCAR, Boulder, CO
- Zahed F, Etemad-Shahidi A, Jabbari E (2008) Modeling of salinity intrusion under different hydrological condition in Arvand River Estuary. *Can J Civ Eng* 35:1476–1480

